Structure and transport properties of liquid clusters in a drying porous medium

H. P. Huinink,* L. Pel, and M. A. J. Michels
Department of Applied Physics, Technische Universiteit Eindhoven, P.O. Box 513, 5600 MB Eindhoven, The Netherlands
(Received 28 May 2003; published 20 November 2003)

The structure and transport properties of drying water clusters in porous media have been studied with a site-bond invasion percolation (IP) model. In this model an invader (air) enters a lattice (porous network) filled with defender (water) via a sequence of invasion steps. The decision to invade a site (pore) is made on the basis of the resistance of the bonds (throats). It is found that the backbone of the defender network and its transport properties are the same as in ordinary percolation (OP). In particular the strength exponent of the backbone $\beta_B = 0.99 \pm 0.03$, the correlation length exponent $\nu = 0.88$, and the conductivity exponent $\mu = 1.99 \pm 0.04$ are the same as in OP. The total network deviates from networks generated with OP: on short length scales the formation of branches is suppressed because pores with many empty neighbors are preferentially invaded. The differences between our IP results and the outcomes of OP are a consequence of the invasion mechanism. This makes clear that the details of the invasion process are important for understanding the transport properties in a drying network.

DOI: 10.1103/PhysRevE.68.056114 PACS number(s): 64.60.Ak, 47.53.+n, 47.55.Mh

I. INTRODUCTION

Salt weathering is an important cause in deterioration of buildings, monuments, and natural rocks [1]. Salt weathering processes are always accompanied by drying phenomena [2,3], and these play an important role because they influence the mobility of ions inside the porous medium. The structure of the network of liquid-filled pores determines the mobility of the ions and depends on the stage of the drying process. Therefore, to understand the diffusivity of ions, knowledge on the evolution of drying water networks is needed. For our particular problem it is a natural choice to use percolation models. In drying porous media, or more generally in unsaturated porous systems, air and water form clusters and networks by a percolation process.

Much is known of diffusive motions of particles on percolation clusters [4,5]. The important length scale is the characteristic size ξ of the network, i.e., the length scale above which the medium can be considered as homogeneous. When particles travel by Brownian motion over distances larger than ξ, their paths obey random-walk statistics and the diffusion process can be described with an effective diffusion coefficient. Motions over distances smaller than ξ cannot be described with random walk statistics and the diffusion is called anomalous; due to the fractal properties of the network at length scales below ξ the diffusion slows down. It has to be remarked that most diffusion studies have been done with clusters generated with ordinary percolation (OP, also called random percolation). Whether or not OP correctly describes the structure of the water network during a drying process is still an open issue.

The invasion percolation (IP) model seems to be a more natural choice for the process of interest [6–8]. In IP an invader fluid (air in the case of drying) enters the porous medium from one single point or side of the system. IP models have been of great value for understanding the relation between multiphase-flow phenomena and pore-scale events [9–16]. It has been proven that the ingress of air during an evaporation process follows IP-type rules [17,18]. When a three-dimensional (3D) system dries slowly and gravity does not play an important role, a standard IP model successfully describes the sequence of invasions down to liquid contents of about 20–30 % [19].

As already mentioned, we want to investigate the diffusion in the water phase during the drying of a 3D porous system. Therefore, we are mainly interested in the structure and transport properties of the defender clusters. IP models are used for more than 20 yrs, but most efforts have been put in the study of the invader phase and little attention has been paid to the structure of the defender network and clusters. In this study, we want to investigate the defender network: its structure and transport properties. Results will be compared with the outcomes of OP models.

This paper is organized as follows. In Sec. II we discuss the relation between the drying of a porous medium and IP, the connection between IP and OP, the behavior of networks near a percolation threshold, and the site-bond IP model used in this study. In Sec. III model calculations will be discussed. First, the structural and transport properties of the water network at the fragmentation point are analyzed in detail. Further, we discuss how these networks behave away from the fragmentation point. In Sec. IV the conclusions will be drawn.

II. THEORY

A. Drying of three-dimensional systems

In the case that capillary forces dominate over viscous and buoyancy forces, the drying of the 3D porous medium passes through two distinct stages, which can be observed when the drying rate is measured as a function of time [20]. In the first period the drying rate is constant and this regime is therefore called the constant-rate period. In this regime the water is uniformly distributed throughout the sample [21,22]

*Author to whom correspondence should be addressed. Email address: h.p.huinink@tue.nl.

and the rate-limiting step for the drying process is the vapor transport in the boundary layer outside the material. When the water content is at 20–30 % of its initial value, the drying rate starts to decrease. This regime is called the falling-rate period: a front in the water saturation develops, which moves inward. In the falling-rate regime the drying rate is limited by the vapor transport from the saturation front to the external boundary of the material.

Network simulations have shown that there are two important transition points in 3D: breakthrough and fragmentation [19]. Initially, the medium is completely saturated with liquid. Due to the evaporation, air invades the system. At breakthrough (BT) the air cluster just percolates the whole system. This percolation transition is located in the constant-rate period and is difficult to observe in macroscopic experiments. After the BT both water and air phase form sample-spanning clusters. At some moment the water network breaks up in isolated clusters: the fragmentation point (FP). This point marks the transition from the constant-rate period to the falling-rate period. Due to the finite size of the clusters a front develops in the saturation profile after the FP.

Due to the fact that a sample-spanning water network exists up to the FP, standard IP models can be used up to this point to predict the sequence of invasion events [19]. To be more precise, the ingress of air obeys the rules of IP with trapping. Isolated water clusters in the bulk of the porous matrix are embedded in an atmosphere with a water-vapor density close to the equilibrium value. Therefore, the evaporation rates of isolated clusters are negligible compared to the rate of the spanning cluster (the network). As a result, most invasions take place in the spanning cluster just as it is prescribed by an IP model with trapping. The major advantage of IP simulations over drying simulations (in which vapor transport and invasions in the isolated clusters are taken into account) is that the former are less computationally intensive. Therefore, we will use an IP model to study the structure and the transport properties of the liquid network during drying.

B. Relation with ordinary percolation

An interesting feature of IP is that clusters of the invader fluid (air in a drying process) generated via this algorithm have much in common with clusters formed in an OP process [8,23,24]. The simplest site- or bond-IP models (no trapping) belong to the same universality class as OP. In some cases trapping can cause differences between IP and OP. In 2D trapping lowers the fractal dimension D_f of the percolating cluster [24,25]. In 3D trapping is less important because the percolation points of the invader and defender do not coincide. In 3D trapping can change the backbone of the invader clusters, if the rules of the IP models are such that the formation of closed loops is prevented, see, e.g., Ref. [26].

That the structures of IP and OP clusters are rather similar can be understood as follows. Consider a very large lattice of blue sites that are labeled with random numbers $r \in [0,1]$ chosen from an uniform distribution. In OP we color all sites with $r \leqslant q$ red (q is a value larger than the percolation threshold q^*). As a result we end up with one spanning and a number of isolated clusters of red sites. In IP we also want to color the sites with $r \leqslant q$. Now we start at a specific side of the system. At a certain stage of the painting process, we only color sites red, if they are neighbors of sites painted red in previous invasion steps. As a consequence, we generate one single cluster, which is in contact with at least one side of the system. The structure of this cluster is exactly the same as the structure of the percolating cluster generated with OP and has therefore the same scaling behavior. The main difference between IP and OP is the meaning of q. In OP q is the occupation probability of a site or a bond. In IP q is the acceptance probability, which is the chance that a site or bond will be invaded given that it is positioned near the invader/defender interface. It has been found that for standard site IP the percolation threshold q^* is the same as in OP [8,9], which reflects the close relation between these models. Little is known of the relation between the defender cluster in an IP and an OP clusters. However, it seems that for simple site IP the correlation length ξ of the defender network and q^* behave as in OP [8,24], indicating that they are closely related too.

The similarity between OP and IP is of great value for studying the properties of IP networks. For OP systems scaling relations for a number of properties have been obtained and the values of critical exponents are well documented.

C. Properties near a percolation transition

It is well known that a number properties of a network behave as universal close to a percolation transition. In the case of a defender cluster this percolation transition is the fragmentation point FP. Especially for the OP model these properties have been studied in great detail. Because we want to investigate a drying cluster and compare its behavior with that of OP clusters, it is useful to discuss briefly the behavior of OP networks close the percolation transition. For a detailed discussion we refer the reader to the literature [27,28,4,5]. We restrict the discussion to properties that are of interest within the scope of this paper.

Close to a percolation transition various properties of a network behave as universal. Its correlation length ξ, strength P, and long-time diffusion coefficients D and D' obey simple scaling laws:

$$\xi \propto |q-q^*|^{-\nu}, \tag{1}$$

$$P = \frac{M}{L^d} \propto |q-q^*|^{\beta}, \tag{2}$$

$$D \propto |q-q^*|^{\mu-\beta}, \tag{3}$$

$$D' = PD \propto |q-q^*|^{\mu}. \tag{4}$$

In these relations q, q^*, M, and L are the probability that a site is filled, the value of the percolation threshold, the mass of the network, and the linear system size, respectively. The exponents ν, β, and μ are the correlation length exponent ($\nu = 0.88$ for $d=3$), the strength exponent ($\beta = 0.41$ for $d=3$) and the conductivity exponent ($\mu = 2.0$ for $d=3$), re-

TABLE I. Percolation exponents for $d=3$. The values for the OP model are from the references [5] and [31] (marked with †). The IP values for the defender cluster have been obtained in this study. The exponent ν is not determined explicitly in this study, but $\nu=0.88$ is consistent with all data.

Properties	OP ($d=3$)	IP ($d=3$, defender)
q^*	0.311 (site), 0.249 (bond)	$0.25-0.26$
β	0.41	0.46 ± 0.03
ν	0.88	0.88
D_f	2.53	2.48 ± 0.03
β_B	$0.99^{\dagger}$	0.99 ± 0.03
D_B	$1.87^{\dagger}$	1.87 ± 0.03
μ	2.0	1.99 ± 0.04

spectively. In Table I we have listed the values of these exponents and some other percolation properties.

The use of two diffusion coefficients originates from the fact that two ensembles of diffusing particles can be distinguished [4]: (a) all particles with a diffusivity D and (b) the particles on the spanning network with a diffusivity D'. Relations (3) and (4) hold for times t larger than the time that a particle needs to diffuse over a length ξ. In the remainder of this paper we will only work with the latter diffusion coefficient D'.

In finite systems at the percolation transition the correlation length equals the system size, $\xi=L$. This is useful for obtaining the correct scaling exponents from simulations. By combination of $\xi=L$ with expressions (1)–(4), the following expressions can be obtained:

$$M\propto L^{d-\beta/\nu}=L^{D_f}, \tag{5}$$

$$D'\propto L^{-\mu/\nu}. \tag{6}$$

In Eq. (5) D_f is the fractal dimension and $D_f<d$ ($D_f=2.53$ for $d=3$). By varying L values for the various fractal dimensions and percolation exponents can be obtained from simulations.

Finally we want to remark that similar scaling relations exist for the backbone of the percolating cluster. In this paper P_B, β_B, M_B, and D_B will be used for the strength, the strength exponent, the mass, and the fractal dimension of the backbone, respectively.

D. Simulation model

The pore space is represented as a cubic network of dimensions $L\times L\times 2L$ with a grid spacing a. Periodic boundaries are applied in the directions perpendicular to the $L\times 2L$ sides of the network. The nodes and bonds of the network represent the pore bodies and pore throats, respectively. It is assumed that the volume is in the pore bodies and the resistance in the throats. To keep the problem as simple as possible, we assume that all pore bodies have equal size. The radii r of the throats are assigned randomly from a uniform distribution with a width Δ and a mean $\overline{r}$.

Initially, the pore space is saturated with a wetting defender fluid, i.e., water. The invader fluid, air in the case of drying, enters the system at one of the $L\times L$ sides. At each simulation step we identify the throats lying at the invader/defender interface (throats which connect pore bodies filled with invader and defender fluids). The throat with the lowest entry pressure $p_c=2\gamma/r$ (γ is the surface tension) is selected for invasion and the corresponding pore body is emptied. In fact, the decision to invade a site is made by evaluating bond properties. Such an IP model is known as a site-bond IP model [29]. An additional restriction in the model is that isolated clusters cannot be invaded. Isolated water clusters are embedded in a vapor atmosphere with a density close to the equilibrium vapor density. Therefore, these clusters evaporate very slowly compared to the sample-spanning cluster and most invasions will take place in this cluster [19]. So, in fact an IP model with trapping is used. A Hoshen-Kopelman type of method is used to identify the separate clusters [30]. A simulation run is stopped when the FP is reached, i.e., the point where the defender cluster breaks up in isolated clusters.

We calculate the long-time diffusivity D' of the defender network to get information about the transport properties of this network. Throats connecting pore bodies filled with the defender are considered to be open for diffusion, and the local diffusion coefficient equals D_0. In order to obtain D', Kirchhoff's equations are solved with a conjugated gradient method. The backbone of the defender network is identified as the set of throats and bonds which carry current. The masses M of both the defender and invader clusters are calculated in the central $L\times L\times L$ part of the system to minimize the influence of the boundaries. Both D' and M are calculated as averages over various realizations.

III. RESULTS

A. The structure at the fragmentation point

Simulations have been performed for system sizes $L=5-70$. The throat radii r have been distributed according to a uniform distribution with an average value $\overline{r}=a$ and a width $\Delta=0.05a$. For most values of L we have simulated 1000 realizations. For $L=30$, 40, 50, and 70, we have averaged over 792, 489, 10, and 6 realizations, respectively. In Fig. 1 we have visualized a defender network at the FP: all defender sites, the spanning network and its backbone. The percolation properties and exponents obtained via these simulations are listed in Table I.

The masses of the air (invader) cluster at BT, the liquid (defender) cluster at the FP, and the backbone of this latter cluster have been calculated for different system sizes. Results are plotted in Fig. 2. The structure of the invader cluster at BT behaves as expected and its fractal dimension $D_f=2.52\pm0.03$ is close to values reported in the literature for clusters at the percolation transition for both IP and OP models. The behavior of the defender cluster at the FP is more interesting. On larger length scales $L>10$ the cluster behaves as a cluster generated with OP. The fractal dimension $D_f=2.48\pm0.03$ is somewhat lower than reported for OP,

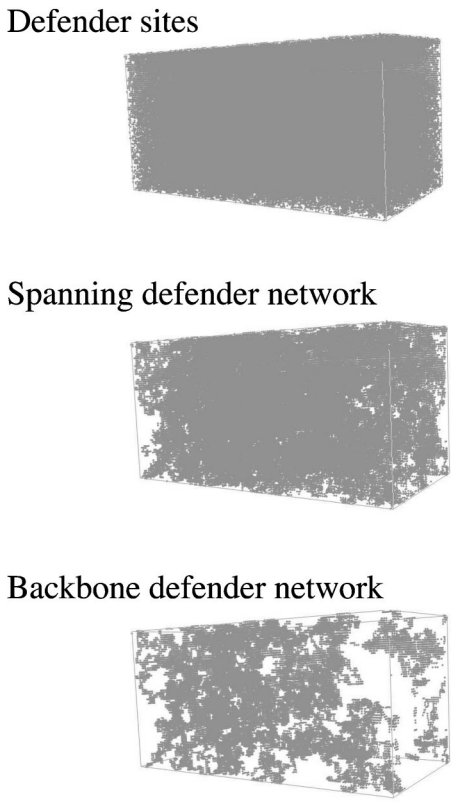

FIG. 1. The defender fluid at the fragmentation point in an $L=70$ system: all sites filled with defender fluid (top), the spanning network (middle), and its backbone (bottom).

2.53, which may be due to the fact that the dataset used for fitting was limited to systems with $10<L\leqslant 40$. In systems with sizes $L\leqslant 10$ the mass of the defender cluster no longer follows this scaling behavior, which indicates that on small length scales the cluster structure deviates from the one generated with an OP or a standard IP algorithms. With decreasing L the mass M of the cluster tends towards the mass of the backbone M_B (Fig. 2), indicating that growth of branches is suppressed on small length scales. This can be understood as follows. In a site-bond IP algorithm the widest throat (bond) is selected to invade a pore body (site). Therefore, the chance that a certain site will be invaded by air increases with increasing number of neighboring sites containing air (the invader fluid). As a consequence, sites of the defender cluster with many empty neighbors are preferentially invaded (emptied) and small-scale roughness is suppressed.

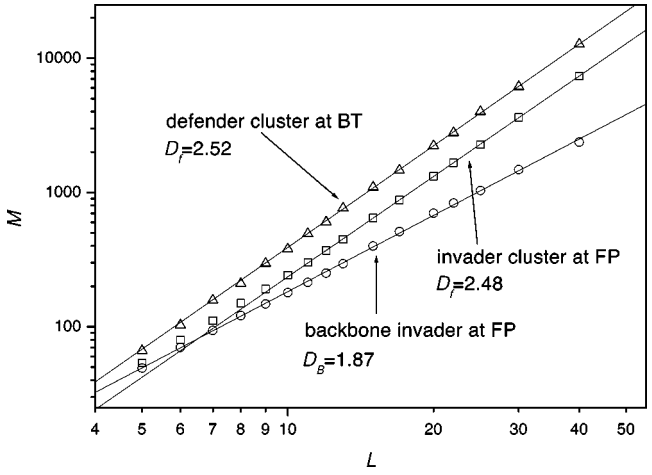

FIG. 2. The masses of: the invader (air) cluster at breakthrough BT ($\triangle$), the defender (liquid) cluster at the fragmentation point FP ($\square$), and the backbone of this defender cluster ($\bigcirc$). The solid lines represent the fits through the data points.

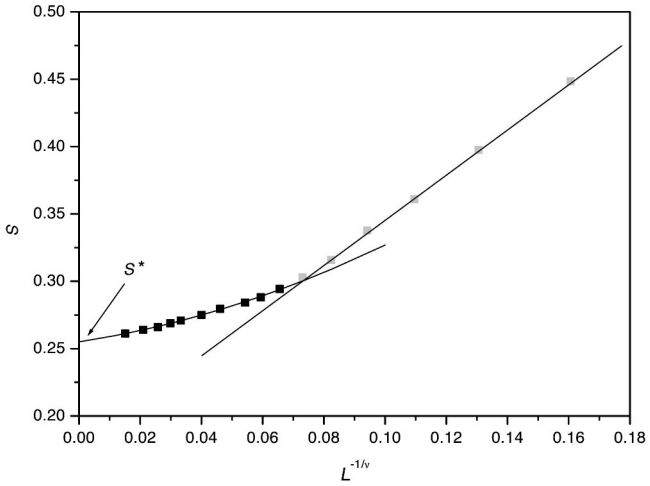

FIG. 3. The liquid saturation S (fraction of sites occupied by the defender fluid) at the fragmentation point FP. In an infinite system $L=\infty$ the defender network breaks up in isolated clusters at $S=S^*$.

The structure of the backbone is not influenced by this subtlety of the site-bond IP algorithm and its mass nicely scales with the system size down to very small values of L. The fractal dimension $D_B\equiv d-\beta_B/\nu=1.87\pm 0.03$ of the backbone is equal to the value obtained with OP (1.87) [31]. This suggests (a) that the correlation length ξ of the defender network behaves as in OP with $\nu=0.88$ and (b) that finite-size scaling leads to an apparent L dependence of the values of β and D_f. On large length scales β equals the normal IP value ($\beta\approx 0.41$), while for $L<10$ β tends towards the backbone value $\beta_B=0.99\pm 0.03$ ($\nu=0.88$). We have tried to extract a relation between ξ and the liquid saturation S (the total number pore bodies filled with defender divided by L^3) by plotting S as a function of $L^{-1/\nu}$, see Fig. 3. Note that $\xi=L$ at the FP. Again two different regimes can be seen. We did not succeed in fitting the data with one single equation for all values of L due to the abrupt change in the slope around $L=10$. The data for $L\leqslant 10$ can be fitted reasonably well with a relation $S\propto L^{-1/\nu}$. Due to a lack of data points for large L, it is hard to come up with an accurate relation for systems with $L>10$. This part of the curve has been fitted with a parabolic equation, in order to estimate the percolation threshold. By fitting the data we obtain the following expression for the correlation length ξ:

$$\xi=\begin{cases} A|S-S^{\dagger}|^{-\nu}, & \xi\leqslant 10 \\ \left|\sqrt{C^2+F(S-S^*)}-C\right|^{-\nu} & \xi>10, \end{cases} \tag{7}$$

where $S^{\dagger}=0.179$, $A=1.57$, $S^*=0.255$, $C=0.047$, and F

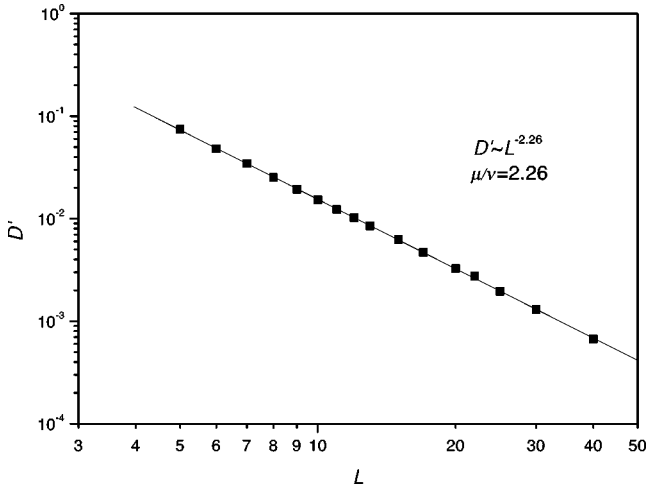

FIG. 4. The diffusion coefficient D' on the spanning cluster at the fragmentation point FP for different system sizes L.

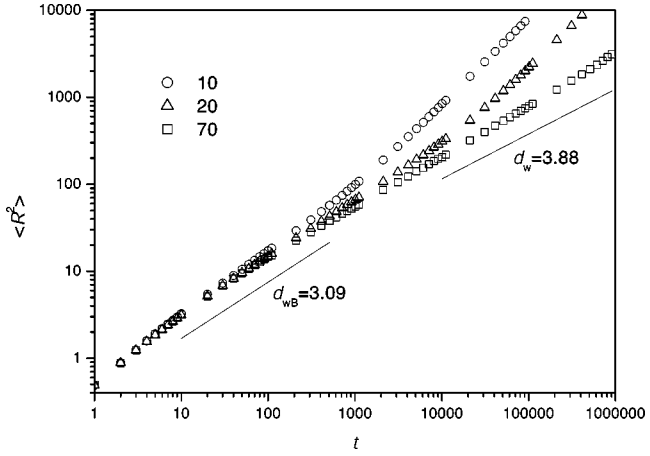

FIG. 5. The behavior of diffusing particles on the spanning defender cluster at the fragmentation point for different system sizes, $L=10$ (○), 20 (Δ), and 70 (□). The lines represent systems with random-walk dimensions of an OP cluster, $d_w=3.88$ [28], and its backbone $d_{wB}=3.09$ [31].

$=0.271$. The quantity S^* is the real percolation threshold and its value is close to that of bond OP, see Table I. It has to be remarked that for a more precise determination of both S^* and of the dependence of ξ on S for $\xi>10$, simulations with larger systems are needed. The actual value of S^* will be in between 0.25 and 0.26. We also expect that such larger calculations will show that a relation $S\propto L^{-1/\nu}$ holds for large L [24]. That a parabolic equation is needed for an accurate fit could be a crossover effect; this would also explain the somewhat low value obtained for the fractal dimension of the defender network $D_f=2.48$ see Table I. The existence of the two regimes is in agreement with the idea that the structure of the defender cluster is different on small and large length scales. The fact that $S\propto L^{-1/\nu}$ for $L\leqslant 10$ seems to confirm the idea that the correlation length of the defender network behaves as in OP, with the expected value $\nu=0.88$.

B. Transport properties at the fragmentation point

As a next step we have calculated the diffusivity D' of ions in the defender phase at the fragmentation point FP. In Fig. 4 we have plotted D' as a function of the system size L. The diffusion coefficient shows nice scaling behavior for all values of L. This is in agreement with the behavior of the backbone, of which the mass could also be fitted with a single power law, see Fig. 2. By fitting the data with Eq. (6) we obtain $\mu/\nu=2.26\pm0.04$ and $\mu=1.99\pm0.04$ ($\nu=0.88$), which is close to the values obtained with OP (Table I). This confirms our ideas regarding the structure of the backbone of the defender cluster: although the defender cluster itself deviates from OP behavior, this deviation is due to the branches. The backbone behaves as in OP and so does the diffusion coefficient D' because it is a property of the backbone of the cluster.

While D' behaves as in OP, diffusion processes on OP clusters and on site-bond IP clusters nevertheless differ for two reasons. First, the diffusion coefficient calculated as an average over all particles, D, equals D'/P [see Eq. (4)] and therefore depends on the structure of the whole defender network. In the previous section we have shown that the structure of this network is different on small and large length scales. Second, we expect that particles will move faster through a network generated with the site-bond IP model than through an OP network. Due to the fact that small branches are suppressed, there will be fewer dead-end traps for the diffusing particles. This will be reflected in the random-walk dimension d_w.

For a few systems ($L=10$, 20, and 70) we have generated random walks and calculated the average squared displacement $\langle R^2\rangle$ of diffusing particles on the percolating defender cluster, see Fig. 5. For $\sqrt{\langle R^2\rangle}\ll L$ all systems behave the same and anomalous diffusion is found, $d_w>2$. Figure 5 indicates that d_w increases with $\langle R^2\rangle$, which is in agreement with the fact that on small length scales the formation of branches is suppressed and the structure of a cluster is more backbonelike. For OP clusters it is known that the random-walk dimension of a cluster ($d_w=3.88$ [28]) is larger than that of its backbone ($d_{wB}=3.09$ [31]). In Fig. 5 the solid lines represent the diffusion behavior on an OP cluster and on the backbone of such a cluster. This confirms the idea that particles diffuse faster on defender clusters generated with site-bond IP rules than on OP clusters because there are fewer traps for the diffusing particles due to the absence of branches on small length scales.

C. Away from the fragmentation point

In the previous sections we have investigated the structural and transport properties of the defender network at the FP. According to the theory discussed in Sec. II C, the structure and the transport properties of networks at or away from the FP obey simple scaling laws on length scales below the correlation length ξ. In this section we discuss simulation results for the network properties of the defender cluster as a function of the degree of saturation S, in order to see whether or not this is true for the site-bond IP model. In Fig. 6 we have plotted the structural properties of the defender phase (the masses of the network and its backbone) and the diffu-

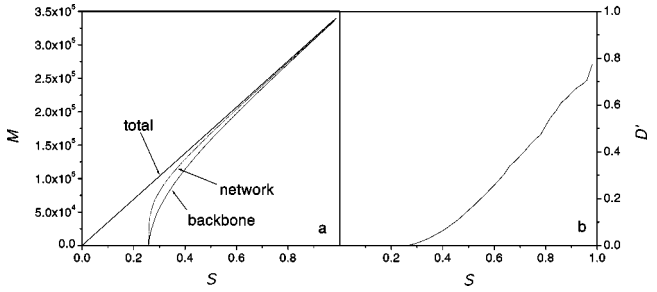

FIG. 6. (a) The masses of the defender network and of its backbone and (b) diffusion coefficient on the former network as a function of the fraction of pores filled by defender fluid S.

sion coefficient D' in a system of size $L=70$ as a function of the defender saturation S. The behavior of the network is as expected. Close to the FP the strength of the network and of its backbone rapidly drop to zero when $S \downarrow S^*$. Therefore $D' \rightarrow 0$ when the system approaches the FP. Close to $S=1$ D' rapidly decreases from 1 to 0.8 with decreasing S. This is due to the fact that the invader (air) enters the system from one side. In the beginning of the invasion process most invasions occur close to the entrance, which creates a relatively ''dry'' surface layer with a high resistance against diffusion.

Results obtained for one single system, as shown in Fig. 6, are instructive, but of little value for a more quantitative analysis because finite-size effects make it difficult to observe power-law relations like Eqs. (2) and (4). Therefore, percolation exponents are generally determined at the percolation threshold by finite-size scaling as we did in the previous sections. Testing whether or not the outcomes also hold away from the FP ($S>S^*$) can again be done with the help of finite-size scaling. Consider a property Y which behaves in an infinite system as

$$Y \propto \xi^{-\lambda/\nu}, \tag{8}$$

where λ is a scaling exponent. In a system of size L the following relation holds for Y [32]:

$$Y = L^{-\lambda/\nu} f((L/\xi)^{1/\nu}), \tag{9}$$

where $f(x)$ is a scaling function with $x \equiv (L/\xi)^{1/\nu}$: $f(x) = \text{const} \times x^{\lambda}$ for $x \gg 1$ and $f(x)=1$ for $x \ll 1$. In our particular case the use of Eq. (9) is complicated by the fact that ξ cannot be described with one single power law for all values of S, see Fig. 3 and Eq. (7).

First, we want to analyze the strength of the backbone $P_B = M_B/L^d$. By using $Y=P_B$, $\lambda=\beta_B$, and relation (9) it can be shown that the scaling function is equal to $M_B L^{-D_B}$. In Fig. 7 we plotted $M_B L^{-D_B}$ as a function of $x=(L/\xi)^{1/\nu}$. In the case that $1 \leqslant \xi \leqslant 10$, Fig. 7(a), most of the data points collapse on a master curve, the solid line, which is given by the relation $f(x)=Cx^{\beta_B}$. Deviations of this master curve are observed for all system sizes when L/ξ approaches L. When the saturation increases, the correlation length decreases. The correlation length saturates at its minimal value, $\xi=1$, which is the distance between two neighboring sites. When $\xi > 10$, Fig. 7(b), the data points again collapse on a single curve, close to the previously obtained master curve $f(x)$

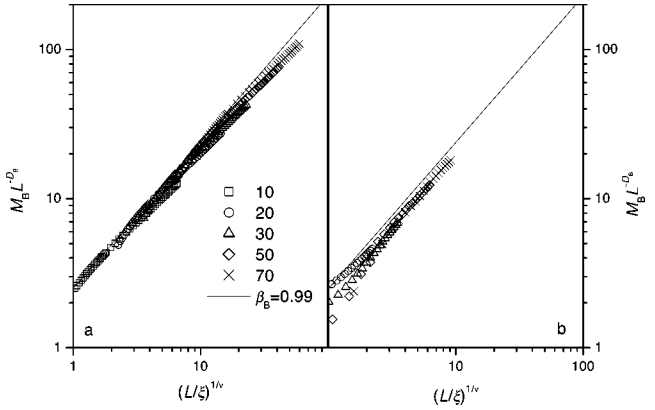

FIG. 7. Finite-size scaling of the backbone mass of the defender cluster; $M_B L^{D_B}$ is equal to the scaling function $f(x)$, where $x=(L/\xi)^{1/\nu}$. The symbols refer to various system sizes: $L=10$ (□), 20 (○), 30 (Δ), 50 (◇), 70 (×). Two expressions for ξ has been used, Eq. (7): (a) the one for $\xi \leqslant 10$ and (b) the one for $\xi > 10$. The solid lines represent a function $f(x)=Cx^{\beta_B}$.

$=Cx^{\beta_B}$. It seems that the data points are now located slightly below the function $f(x)$. Deviations are observed for low values of L/ξ, where S is close to S^*. When S approaches S^*, the correlation length diverges until it saturates at its maximal value $\xi=L$. That in both cases the data points obey a relationship of the form x^{β_B}, confirms that we have found the correct values for D_B and β_B.

By using $Y=D'$, $\lambda=\mu$, and relation (9) it can be shown that the scaling function for diffusivity is equal to $D' L^{\mu/\nu}$. In Fig. 8 we have plotted $D' L^{\mu/\nu}$ as a function of $x=(L/\xi)^{1/\nu}$. In the case that $1 \leqslant \xi \leqslant 10$, Fig. 8a, the data points follow a master curve, which is represented by a solid line and obeys the relation $g(x)=Kx^{\mu}$. For the various systems deviations are observed both for high and low values of L/ξ. Again the deviations for high values of L/ξ result from a saturation of the correlation length at its minimal value, $\xi=1$. The deviations at low L/ξ values seem to be related

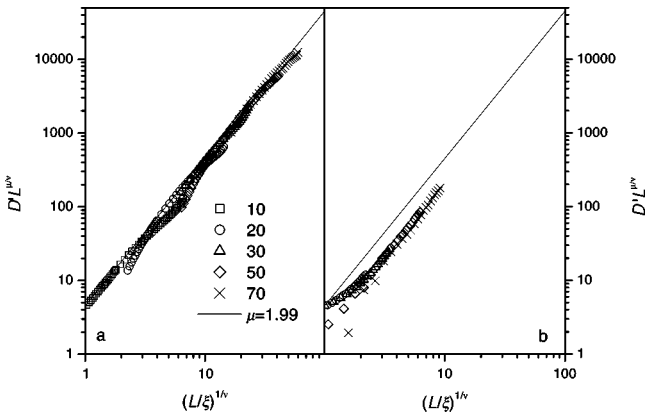

FIG. 8. Finite-size scaling of the diffusion constant of the defender cluster; $D' L^{\mu/\nu}$ is equal to the scaling function $g(x)$, where $x=(L/\xi)^{1/\nu}$. The symbols refer to various system sizes: $L=10$ (□), 20 (○), 30 (Δ), 50 (◇), and 70 (×). Two expressions for ξ has been used, Eq. (7): (a) the one for $\xi \leqslant 10$ and (b) the one for $\xi > 10$. The solid lines represent a function $g(x)=Kx^{\mu}$.

with the behavior at $\xi > 10$. In Fig. 8(b) we have plotted the data for $\xi > 10$ together with the previously obtained relation $g(x) = Kx^{\mu}$ (the solid line). Also here most of the data points collapse on a single curve. The observed deviations at low values of L/ξ are due to the fact that the correlation length saturates at its maximal value, $\xi = L$. An interesting feature of Fig. 8(b) is that the master curve follows a scaling-law x^{μ}, but is shifted significantly below the function $g(x) = Kx^{\mu}$. Until now we do not have a clear explanation for this feature. It might be that our expression for ξ, Eq. (7), is not accurate enough. However, the fact that in both cases the data points obey a relationship of the form x^{μ}, seems to confirm that we have indeed found the correct value for the conduction exponent μ.

IV. CONCLUSIONS

We have studied the structure and the transport properties of a drying water network by using a site-bond invasion percolation IP model, in which the invader and defender represent air and water, respectively. The outcomes of the simulations have been compared with well-known results of OP.

The site-bond IP simulations predict that the backbone of a defender network and its transport properties are the same as in OP. The strength exponent of the backbone $\beta_B = 0.99 \pm 0.03$, the correlation length exponent $\nu = 0.88$, and the conductivity exponent $\mu = 1.99 \pm 0.04$ are almost the same as in OP. However, the behavior of the total network deviates from that of networks generated with OP. On short length scales (when the correlation length $\xi \leqslant 10$) the formation of branches is suppressed in the site-bond IP model, due to the fact that pores with many empty neighbors are preferentially invaded. On larger length scales branches are not suppressed and the network behaves in OP, $\beta = 0.41$. The differences between our IP results and the outcomes of OP are a consequence of the invasion mechanism used in the IP model: sites (pores) are invaded by evaluation of values (radii) assigned to the bonds (throats).

We have found that the mobility of ions on a network generated with the site-bond IP model is higher than that from an OP model. Due to the fact that the defender network lacks small branches, there are fewer traps for diffusing particles. This makes clear that the details of the invasion process are important for understanding the transport properties in a drying network.

ACKNOWLEDGMENT

This project was financially supported by the Dutch Technology Foundation (STW).

[1] A. Goudie and H. Viles, *Salt Weathering Hazards* (Wiley, Chichester, 1997).
[2] S.Z. Lewin, in *Conservation of Historic Stone Buildings and Monuments*, edited by the Committee on Historic Stone Buildings and Monuments (National Acad. Press, Washington D.C., 1980), p. 180.
[3] L. Pel, H.P. Huinink, and K. Kopinga, Appl. Phys. Lett. **81**, 2893 (2002).
[4] S. Havlin and D. Avraham, Adv. Phys. **36**, 695 (1987).
[5] D. Stauffer and A. Aharony, *Introduction to Percolation Theory*, 2nd ed. (Taylor & Francis, London, 1994).
[6] R. Lenormand and S. Bories, C. R. Seances Acad. Sci., Ser. B **291**, 279 (1980).
[7] R. Chandler, J. Koplik, K. Lerman, and J.F. Willemsen, J. Fluid Mech. **119**, 24 (1982).
[8] D. Wilkinson and J.F. Willemsen, J. Phys. A **16**, 3365 (1983).
[9] D. Wilkinson, Phys. Rev. A **30**, 520 (1984).
[10] D. Wilkinson, Phys. Rev. A **34**, 1380 (1986).
[11] J.P. Hulin, E. Clement, C. Baudet, J.F. Gouyet and M. Rosso, Phys. Rev. Lett. **61**, 333 (1988).
[12] A. Birovljev, L. Furuberg, J. Feder, T. Jossang, K.J. Maloy, and A. Aharony, Phys. Rev. Lett. **67**, 584 (1991).
[13] V. Frette, J. Feder, T. Jossang, and P. Meakin, Phys. Rev. Lett. **68**, 3164 (1992).
[14] M. Chaouche, N. Rakotomalala, D. Salin, B. Xu, and Y.C. Yortsos, Phys. Rev. E **49**, 4133 (1994).
[15] Y.C. Yortsos, B. Xu, and D. Salin, Phys. Rev. Lett. **79**, 4581 (1997).
[16] H.P. Huinink and M.A.J. Michels, Phys. Rev. E **66**, 046301 (2002).
[17] M. Prat, Int. J. Multiphase Flow **19**, 691 (1993).
[18] M. Prat, Int. J. Multiphase Flow **21**, 875 (1995).
[19] Y. Le Bray and M. Prat, Int. J. Heat Mass Transfer **42**, 4207 (1999).
[20] J. van Brakel, in *Advances in Drying*, edited by A.S. Mujumdar (Hemisphere, Washington, D.C., 1980), Vol. 1, p.217.
[21] L. Pel, A.A.J. Ketelaars, O.C.G. Adan, and A.A. van Well, Int. J. Heat Mass Transfer **36**, 1261 (1993).
[22] L. Pel, H. Brocken, and K. Kopinga, Int. J. Heat Mass Transfer **39**, 1273 (1996).
[23] D. Wilkinson and M. Barsony, J. Phys. A **17**, L129 (1984).
[24] M.M. Dias and D. Wilkinson, J. Phys. A **19**, 3131 (1986).
[25] R. Lenormand and C. Zarcone, Phys. Rev. Lett. **54**, 2226 (1985).
[26] A.P. Sheppard, M.A. Knackstedt, W.V. Pinczewski, and M. Sahimi, J. Phys. A **32**, L521 (1999).
[27] M. Sahimi, *Flow and Transport in Porous Media and Fractured Rock* (VCH, Weinheim, 1995).
[28] D. Avraham and S. Havlin, *Diffusion and Reactions in Fractals and Disordered Systems* (Cambridge University Press, Cambridge, 2000).
[29] M. Sahimi, M. Hashemi, and J. Ghassemzadeh, Physica A **260**, 231 (1998).
[30] K. Binder and D.W. Heermann, *Monte Carlo Simulation in Statistical Physics*, 3rd ed. (Springer, Berlin, 1997).
[31] M. Porto, A. Bunde, S. Havlin, and H.E. Roman, Phys. Rev. E **56**, 1667 (1997).
[32] M.E. Fisher, in *Critical Phenomena*, Proceedings of the International School of Physics ''Enrico Fermi'' Course 51, edited by M.S. Green (Academic, New York, 1971).